Int. J. Heat Mass Transfer. Vol. 28, No. 6, pp. 1115–1129, 1985
Printed in Great Britain

0017–9310/85 $3.00 + 0.00
Pergamon Press Ltd.

Boiling burnout and flow instabilities for water flowing in a round tube under atmospheric pressure

KAICHIRO MISHIMA, HIEDEAKI NISHIHARA
Research Reactor Institute, Kyoto University, Kumatori, Osaka 590-04 Japan

and

ITARU MICHIYOSHI
Department of Nuclear Engineering, Kyoto University, Yoshida-honmachi, Sakyo-ku, Kyoto 606 Japan

(*Received* 27 *June* 1984 *and in final form* 14 *November* 1984)

Abstract—In order to study critical heat flux (CHF) at low mass velocities, flow stagnation and flow reversal conditions, an experiment has been performed with water flowing in a round tube at atmospheric pressure. The main emphasis was given to the effects of buoyancy (i.e. upflow and downflow), upstream compressibility and inlet valve throttling. The reslts indicated that the CHF due to flow instabilities could be remarkably lower than the stable-flow CHF. It is also pointed out that the lower boundary of unstable-flow CHF corresponds to the annular-flow boundary or the flooding CHF.

1. INTRODUCTION

NUMEROUS and extensive works have been performed on burnout phenomena in round tubes in the last quarter of a century. A number of comprehensive reviews on the subject also have been published [1–8]. Since the critical heat flux (CHF) problem has been investigated particularly in the development of nuclear reactors in which the main concerns have been the maximum power extractable from the reactor, much effort has been devoted to the development of the design correlations for CHF predictions at such high-flow-rate/high-pressure conditions as expected in light water reactors.

On the other hand, it is only recently that emphasis has been given to CHF at very low mass velocities, flow stagnation and flow reversal conditions, of interest for steam generators with natural convection and for nuclear reactors in accident conditions, such as a loss-of-coolant accident (LOCA) [5, 6]. There exist several CHF correlations [9–12] which are applicable for CHF at low flow rates. Barnard *et al.* [13] investigated CHF for Freon-113 flowing in tubes near atmospheric pressure and at mass velocities from zero to 320 kg m^{-2} s^{-1}. They observed that CHF at zero inlet mass velocity occurred due to flooding or pool-boiling CHF. For low mass velocities, CHF occurred due to complete evaporation or entrainment-limited mechanism.

It is noted that the above mentioned results for upflow were obtained under stable-flow conditions. However, it is generally known that boiling channels are subject to various flow instabilities, which may be the cause of premature burnout [14–21]. Lowdermilk *et al.* [14] showed that the flow became unstable and consequently the CHF decreased with larger upstream compressibility and less inlet throttling. Maulbetsch and Griffith [18] studied both flow excursion and pressure-drop oscillations. It was shown that the upstream compressibility worked as an energy storage mechanism in pressure-drop oscillations and those flow instabilities could be effectively controlled by providing a large inlet throttling just prior to the heated section.

There is only a little literature on CHF for downflow [22–24]. Blumenkrantz and Gambill [22] observed downflow CHF several-fold lower than upflow CHF at very low mass velocities of water. Downflow CHF obtained by Cumo *et al.* [23] for Freon-12 was about 11% lower than upflow CHF with the conditions otherwise the same.

Although a large number of investigations have been performed on CHF for water flowing in round tubes, the LOCA characteristics of low velocity, flow stagnation, and flow reversal, are not well understood and reference steady-state critical-heat-flux data for low velocities and pressures are needed, as stated by Bergles [5]. In view of these, experiments have been performed with water flowing in a round tube at low-flow-rate and low-pressure conditions to study the effects on CHF, of buoyancy (i.e. upflow and downflow), upstream compressibility (upper and lower plena) and inlet valve throttling. Critical heat flux at complete bottom blockage also has been measured. Furthermore, CHF vs mass-velocity curves are compared with observed flow-stability boundaries at given inlet water temperatures.

NOMENCLATURE

A	flow area
A_H	heated area
C_0	distribution parameter
D	tube diameter
f_l	liquid phase friction factor
f_m	two-phase friction factor
G	mass velocity
G^*	non-dimensional mass velocity defined by equation (7)
G_c	critical mass velocity to cause bubble stagnation
g	gravity
h	enthalpy
h_{fg}	latent heat of vaporization
Δh_i	inlet subcooling (enthalpy)
K_e	exit resistance coefficient
K_i	inlet resistance coefficient
L	length
L_{NB}	length of the non-boiling region
L_H	heated length
L_u	length of unheated region
p	pressure
Δp	pressure drop
Δp_A	pressure loss due to acceleration
Δp_e	pressure loss at the exit
Δp_{ext}	external pressure drop (supply pressure drop)
Δp_g	pressure drop due to gravity
Δp_{int}	internal pressure drop (system-demand pressure drop)
Δp_{pump}	pump head
Δp_{TPF}	frictional pressure loss of two-phase flow
$\left(\frac{\partial \Delta p}{\partial G}\right)_{int}$	slope of the internal pressure-drop vs mass velocity curve
$\left(\frac{\partial \Delta p}{\partial G}\right)_{ext}$	slope of the external pressure-drop vs mass velocity curve
q	heat flux
q_c	critical heat flux
q_{cF}	critical heat flux due to flooding
q^*	non-dimensional heat flux defined by equation (6)
Re_l	liquid Reynolds number
T_{in}	inlet water temperature
x_e	exit quality.

Greek symbols

α	void fraction
α_e	void fraction at the exit of the heated section
α_H	average void fraction in the heated section
ρ_k	density of k phase (k = g or l)
ρ_{li}	density of the liquid at the inlet
$\Delta\rho$	difference of the density between two phases
μ_k	viscosity of k phase (k = g or l)
$\Delta\mu$	difference of the viscosity between the two phases
λ	length scale of the Taylor wave defined by equation (8)
σ	surface tension.

2. EXPERIMENT

2.1. *Test section*

The test section is made up of a 6-mm ID, 1-mm thick stainless-steel tube as shown in Fig. 1. A copper electrode is silver-soldered to each end of the test section. The length of the heated section is 344 mm. The test section is mounted in the loop with suitable fittings and Teflon bushing as electrical insulator. Ten chromel–alumel thermocouples are spot-welded onto the outside wall of the stainless steel tube. The thermocouple locations are shown in Fig. 1. These thermocouples are connected to burnout detectors. The stainless steel tube is heated electrically by a D.C. power supply and water flows inside. The whole test section is thermally insulated with asbestos ribbon.

2.2. *Test loop*

The test loop consists of a test section, a downcomer (water tank), a bypass, a circulating pump, flow control valves, three turbine flowmeters and a pipeline connecting these components as shown in Fig. 2. An upper and a lower plenum and a surge tank are mounted when necessary. The loop is filled with ion-exchanged water, which was degassed by boiling prior to the experiment. Water is circulated by a centrifugal pump whose characteristic is known. The flow orientation in the test section can be set either upward or downward using four stop valves (V2, V3, V4 and V5) in the loop.

Three geometrical arrangements for the test section were employed. In the first series of experiments, the test section was mounted in the loop simply using standard tube fittings and joints in order that there remained as small a compressible volume as possible. A valve (V6) was installed at the bottom of the test section which served for inlet throttling in an upflow. Since no valve was at the top, the one just behind the flowmeter (V1) was used for inlet throttling in a downflow.

The second series of experiments was conducted with a plenum at the top and the bottom of the test section. The volume of the plenum is 1077 cm^3. It should be noted that some amount of non-condensable gas probably remains in the upper plenum during experiment.

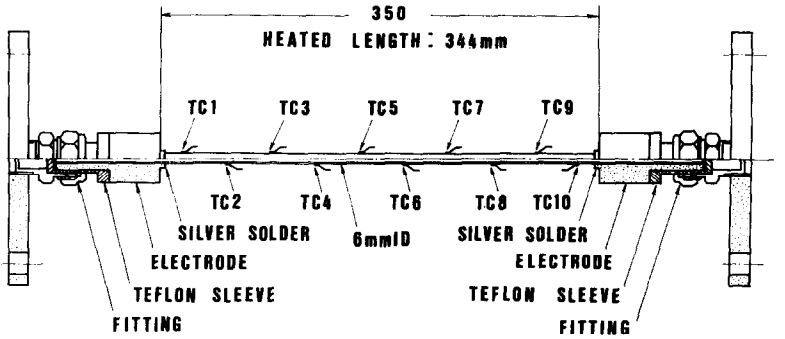

FIG. 1. Test section with round tube heater.

In the third series, a surge tank was connected to the loop upstream of the test section. The volume of the surge tank was about 300 cm^3, but the volume of air in it was changeable.

2.3. *Instrumentation*

The flow rate to the test section was measured with two turbine flowmeters installed parallel to each other in the loop. The electrical outputs from these turbine flowmeters were recorded on a strip chart which enabled us to read the average flow rate as well as to observe the fluctuations.

The water temperatures were measured at the inlet and outlet of the test section, downstream of the flowmeters and in the downcomer with chromel–alumel thermocouples. The heated-wall temperatures were measured with 10 chromel–alumel thermocouples spot-welded onto the heater as mentioned before. All these temperatures were also recorded on a strip chart or with a digital printer.

The pressure in the loop was measured with a Bourdon-tube type gauge installed in the upstream of the test section.

2.4. *Test procedure*

Prior to the experiment, the water in the loop was circulated and boiled for about half an hour for degassing, since the existence of non-condensable gas reduces the CHF considerably. Then the valves were set to obtain the desired flow orientation.

The flow rate was regulated in two ways, namely, either by inlet-valve throttling with all the bypass closed or by throttling the valve downstream of the flowmeters with the inlet valve and the bypass valve open. The former case corresponds to a 'stiff' system though not completely stiff, whereas the latter case corresponds to a 'soft' system.

Critical heat flux was measured at given flow rates and inlet water temperatures. The inlet water temperature was kept constant by using the cooling pipe in the downcomer and the heat input to the test section. The exit pressure was always kept near atmospheric by keeping the relief valve open on the top of the downcomer during the experiment. At each given flow rate, the power to the test section was gradually increased by small steps until a burnout occurred.

The determination of the occurrence of burnout is

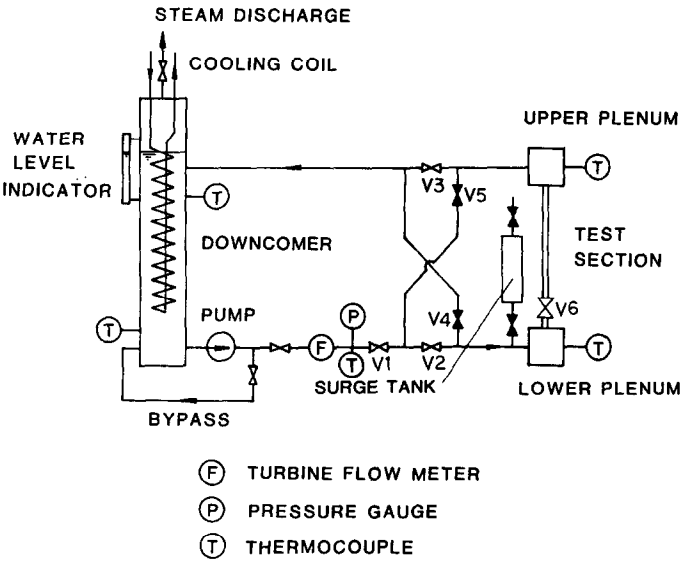

FIG. 2. Schematic showing of the test loop employed in the round tube experiment.

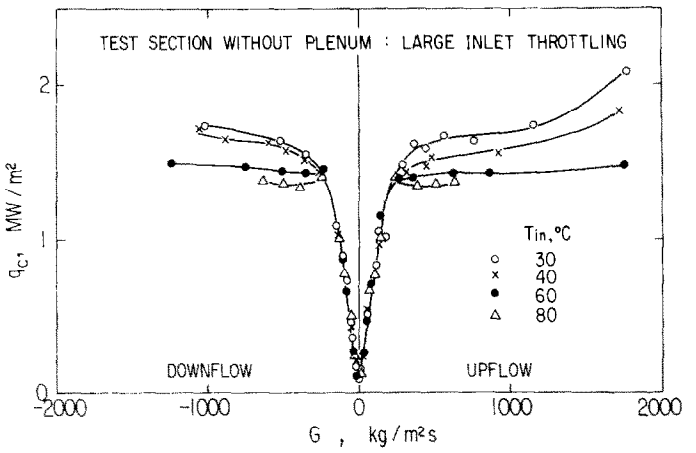

FIG. 3. Overall behavior of CHF as a function of mass velocity for the test section without plenum under stiff condition.

based on the actuation of any one of the burnout detectors, which actuate a relay to switch off the power to the test section as soon as the wall temperatures rise beyond a preset value due to the occurrence of burnout. The preset levels of the detectors were so changed in each run as to trip the circuit properly due to the burnout. Since the wall temperatures were recorded on a strip chart, the occurrence of burnout was observed also from the abrupt increase in the temperature traces.

The heat flux was calculated from the voltage drops across the test section and the calibrated on-line shunt of the power supply assuming a uniform heat flux. The critical heat flux is defined by the heat flux just before the occurrence of rapid temperature excursion.

As will be described later various flow instabilities were encountered. In such cases as the instability directly resulted in burnout, the flow rate corresponding to the CHF was determined by the readings just before the occurrence of the instability. However, there were other cases in which the flow rate decreased to another meta-stable point and held at that level for a while before burnout resulted. In those cases, the CHF data were plotted in two ways, i.e. CHF vs the initial flow rate and CHF vs the flow rate just prior to the burnout.

3. RESULTS AND DISCUSSIONS

3.1. *Overall behavior of CHF*

The overall behavior of CHF as a function of mass velocity is shown in Fig. 3 for the test section without plenum under 'stiff' conditions, i.e. with large inlet throttling. Here, the positive and the negative mass velocities denote upflow and downflow, respectively, while zero inlet mass velocity means the complete blockage of the test channel at the bottom.

It can be seen from the figure that the curves are almost symmetrical about the line with zero mass velocity, which indicates that the effect of buoyancy is

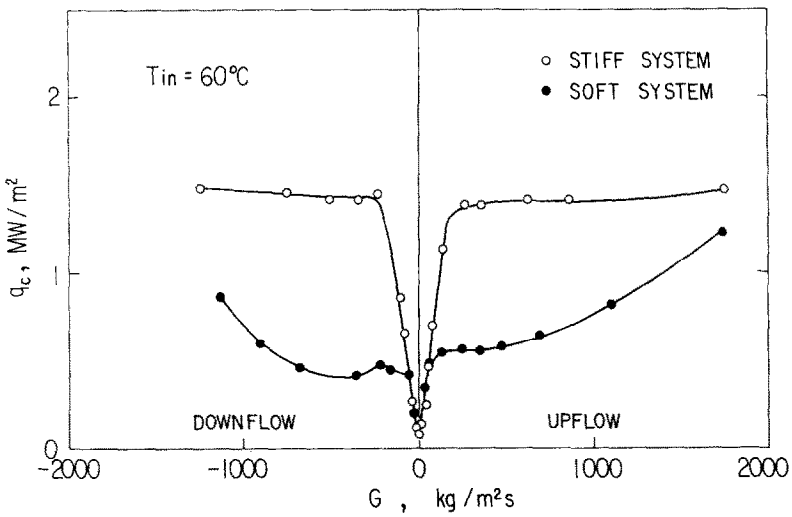

FIG. 4. Effects of inlet throttling on the overall behavior of CHF.

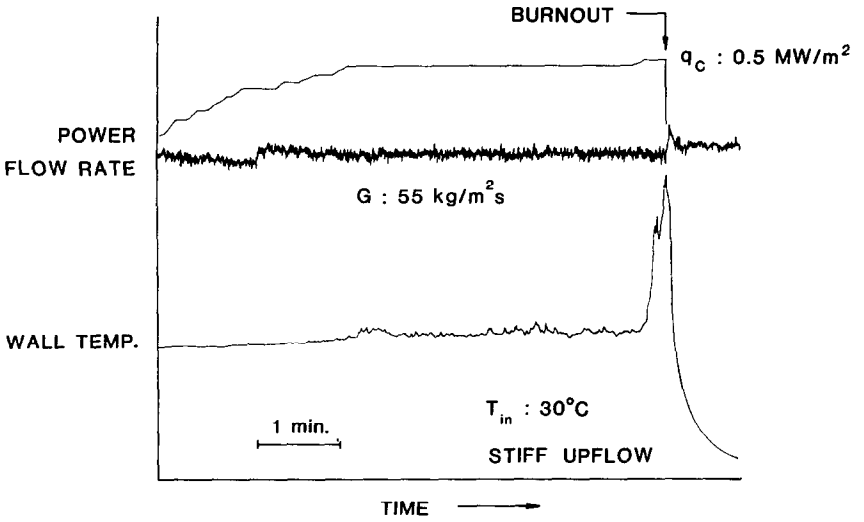

FIG. 5(a). Typical traces at stable-flow burnout.

small for a stiff system. In both upflow and downflow, CHF increases linearly as the mass velocity increases at very low mass velocities. There is a minimum in CHF (ranging from 0.06 to 0.08 MW m^{-2}) at zero inlet mass velocity. It has been pointed out that CHF at zero inlet mass velocity occurs due to flooding [25].

The effect of inlet water temperature is small in this range of parameters. However, at high mass velocities (namely, larger than 200 kg m^{-2} s^{-1}), the gradient of the curves decreases remarkably and the effect of inlet water temperature becomes obvious. At the highest mass velocities, there are some indications that the gradient of the curves increases again with increasing mass velocity.

It has been recognized that in a 'soft' system, flow instabilities may cause CHF to decrease substantially. Figure 4 exemplifies the premature burnout due to flow instabilities when the system is operated with less inlet restriction. The reduction in CHF is larger at lower mass velocities. However, at the lowest mass velocities, two curves appear to merge. This may be attributed mainly to the larger pressure drop across the turbine flowmeter compared to the pressure drop in the heated section for very low flow measurement. The figure also shows that the curve for the soft system is not symmetrical but the CHF is lower for downflow, which indicates that the effect of buoyancy becomes important at very low flow rates.

The flow instabilities prior to burnout were observed in flow rate traces. A typical flow rate trace of stable flow which resulted in a burnout is shown in Fig. 5(a). A flow rate trace of unstable burnout is presented in Fig. 5(b). The amplitude of the fluctuation in the flow rate is much larger in the latter case in which the burnout occurred due to unstable flow. The amplitude of the flow rate trace increases with increasing power to the test section. Figure 6 shows the variation of root-mean-square (r.m.s.) amplitude of the output from the flowmeter with increasing heat flux at given mass velocities. The effect of inlet throttling is also shown there. The r.m.s. amplitude of the flow rate increases sharply just before the occurrence of burnout and the sharp increase in the amplitude occurs at lower heat flux in a soft system.

When the flow rate and the heat flux is relatively high, a small increase in heat flux in some cases causes a sudden large decrease in flow rate. The decrease in flow

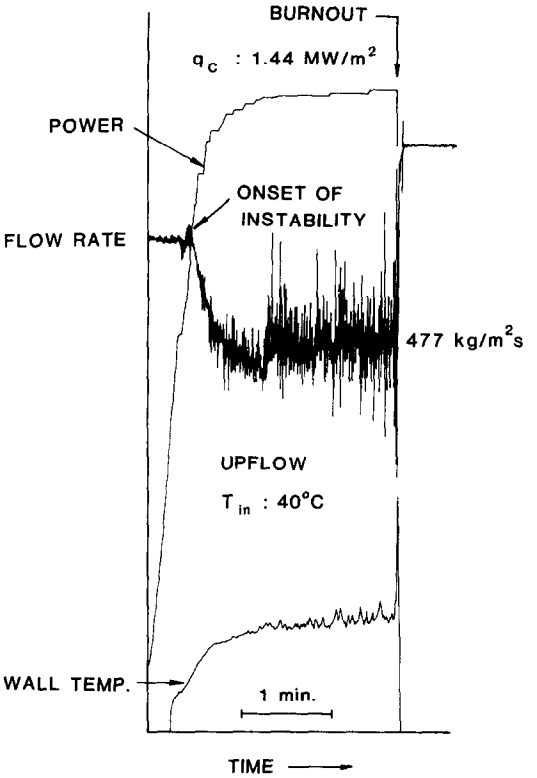

FIG. 5(b). Example of the traces for burnout associated with flow instabilities (density wave oscillations).

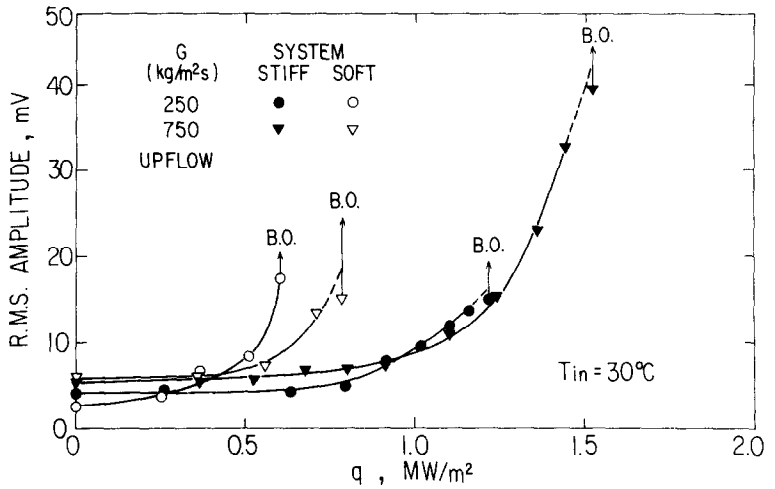

FIG. 6. Effect of inlet throttling on the r.m.s. amplitude of the flow meter output as a function of heat flux.

rate occurs in a non-recurrent manner leading to a burnout as shown in Fig. 7. This is interpreted as an example of burnout due to flow excursion.

The effect of buoyancy on the CHF appears to be remarkable in the test section with upper and lower plena, as illustrated in Fig. 8. In this case, the bypass was closed and the valve V1 in Fig. 2 was used for inlet throttling both in upflow and downflow. In upflow, the curves for CHF vs mass velocity are almost unchanged from those for stiff condition. However, the curves for downflow appears to be entirely different. Figure 8 shows that the critical heat flux remains low up to the mass velocity of about 200 kg m^{-2} s^{-1}, beyond which the gradient of the curves increases. At high mass velocities, however, the gradient of the curves decreases again. From the visual observation in the experiment conducted with rectangular channels [25], CHF at very low downflow is attributed to the bubble stagnation in the heated section. The critical mass velocity to stagnate bubbles is estimated from the bubble drift velocity in the churn flow regime [26]. The resulting equation becomes

$$G_c = -\sqrt{2}(\rho_l^2 \sigma g \Delta\rho)^{1/4}/C_0, \quad (1)$$

where the negative sign represents downflow and the distribution parameter C_0 for a round tube is given by [26]

$$C_0 = 1.2 - 0.2\sqrt{\rho_g/\rho_l}. \quad (2)$$

Using equation (1), the critical mass velocity to stagnate bubbles in the present system becomes -179 kg m^{-2} s^{-1}, which roughly agrees with the mass velocity at which the curves change their gradient as shown in Fig. 8.

When the inlet throttling (V1) is small in upflow, the CHF results are the same as those for the soft system without plena. Hence, the effect of plenum is not evident in upflow, whereas it appears to be significant in downflow. The CHF dropped to as much as one-fifth of that for the stiff system without plena in downflow. This may be explained by the destabilizing effect of buoyancy and the upstream compressibility. In fact, there possibly remained a certain amount of gas in the upper plenum which served as an upstream

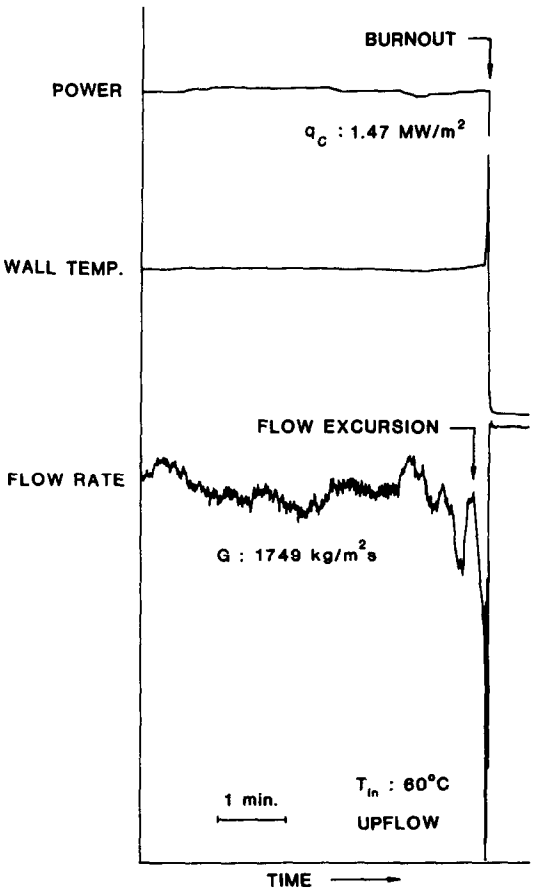

FIG. 7. Example of traces for burnout due to flow excursion.

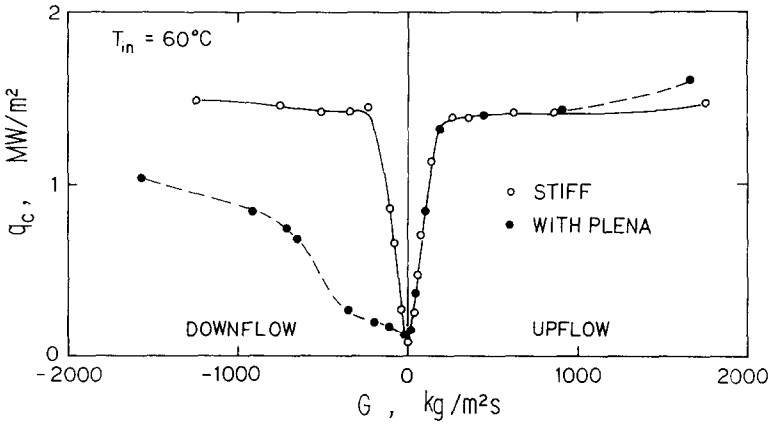

FIG. 8. Overall behavior of CHF as a function of mass velocity for the test section with upper and lower plena in comparison with that for stiff system.

compressibility in the downflow experiment. The above results indicate that the CHF decreases substantially due to unstable flow and the effect of buoyancy destabilizes the flow markedly, leading to further decrease in CHF.

It is known that an upstream compressibility works as an energy storage mechanism to excite pressure-drop oscillations [18]. In order to observe this phenomenon in upflow, a compressible volume (about 140 cm^3 of air in the surge tank) was connected to the loop immediately upstream of the test section and the CHF measured. In some cases, sustained flow oscillations with large amplitudes arose with a small increase in the heat input, and the flow rate dropped to another level gradually as the heat input was increased, keeping the inlet throttling constant. An example is illustrated in Fig. 9. This phenomenon is different from that shown in Fig. 7 in which a burnout initiated directly after the occurrence of flow excursion. The period of the sustained flow oscillations is estimated to be a few seconds and the exit quality is not very high but positive. This type of flow instability as well as the other types which were observed in the present experiment will be discussed later.

The results of CHF in the test section with the compressible volume are shown in Fig. 10. The open triangles in the figure are the data plotted in terms of the initial mass velocity and the solid triangles in terms of the mass velocity just before the burnout when the above mentioned flow instabilities are encountered. It

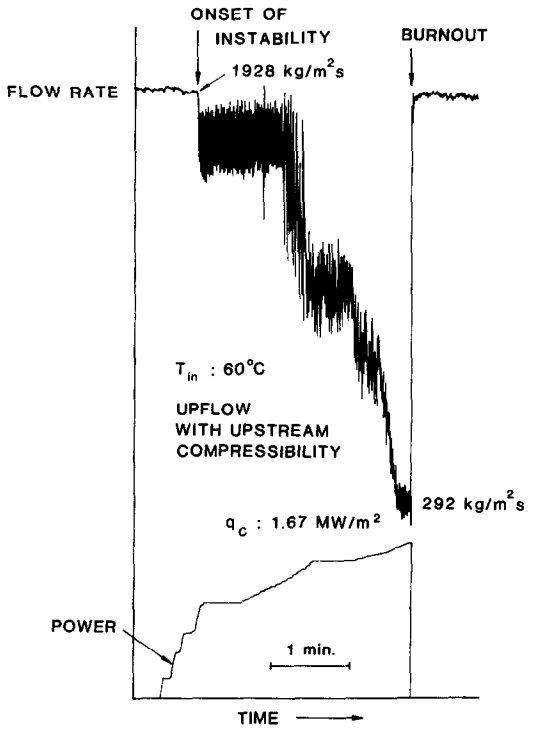

FIG. 9. Complex flow instability in upflow affected by the upstream compressibility.

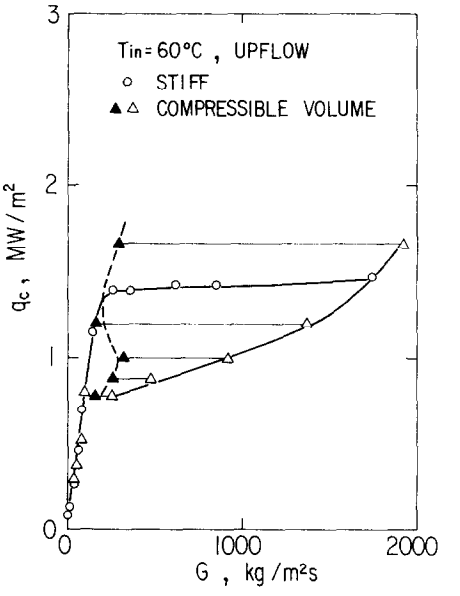

FIG. 10. Effect of compressible volume on CHF for upflow.

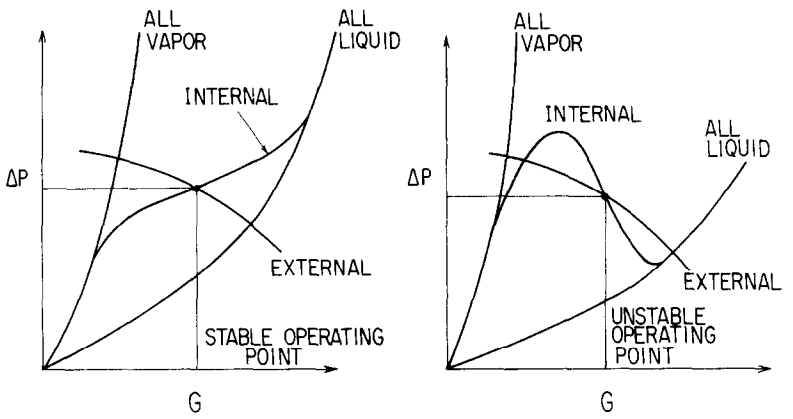

FIG. 11. Stable and unstable pressure-drop characteristics.

is clearly shown that the upstream compressibility causes a burnout at much lower heat flux than the stable CHF in view of initial mass velocity, however, the data approaches the stable CHF in terms of the mass velocity just before the burnout.

3.2. *Relation between the CHF and flow instabilities*

Observed flow instabilities. The CHF observed in the present experiment appears to be considerably affected by various flow instabilities. In that case, the temporary reduction of the flow rate due to instability causes total liquid starvation which may lead to a premature burnout as a consequence.

Two types of flow instabilities were recognized. One is the flow excursion in which a small increase in heat flux at constant valve-throttling causes a sudden non-recurrent reduction of the inlet flow rate and, as a consequence, a burnout. Typical traces illustrating burnout due to a flow excursion have been shown in Fig. 7. The others are oscillatory instabilities. The most common among them are the density-wave oscillation and the pressure-drop oscillation [27–29]. These oscillatory instabilities do not always cause burnout, but the amplitude is so large that it may cause vibrations of the components in the system.

The flow excursion was first analyzed by Ledinegg [30] and so is called the Ledinegg instability. The criterion for the instability was given by

$$\left(\frac{\partial \Delta p}{\partial G}\right)_{\text{int}} < \left(\frac{\partial \Delta p}{\partial G}\right)_{\text{ext}}. \tag{3}$$

This means that the flow excursion occurs when the slope of the internal pressure-drop vs flow-rate curve becomes smaller (more negative) than the external pressure-drop vs flow-rate curve (or pump characteristic). This is illustrated in Fig. 11.

In order to identify the flow excursion, the pressure drops are calculated for a case shown in Fig. 7, in which

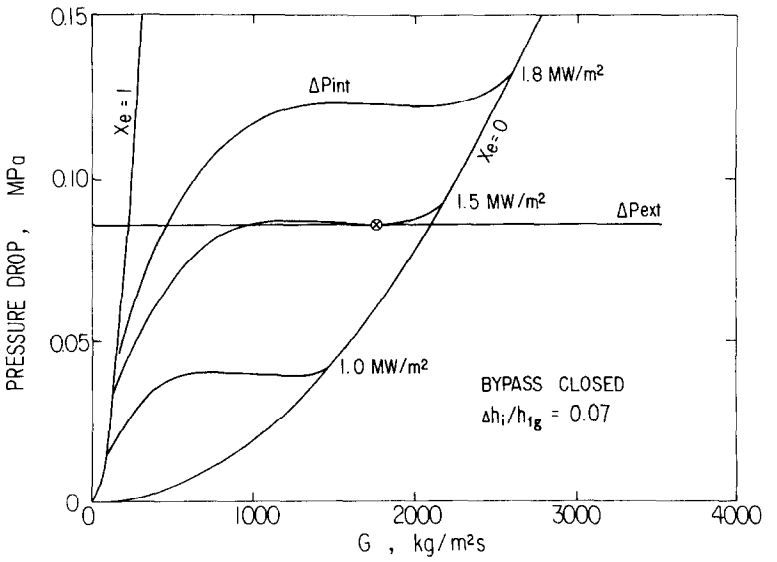

FIG. 12. Example of the pressure-drop vs flow-rate curves for the case shown in Fig. 7 which resulted in a burnout due to flow excursion.

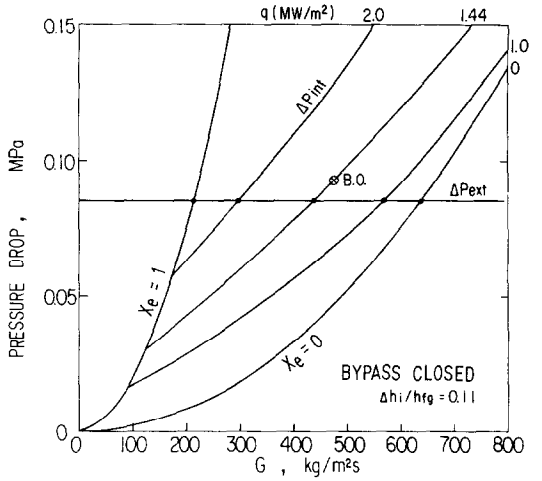

FIG. 13. Example of the pressure-drop vs flow-rate curves for the case shown in Fig. 5(b) in which the density-wave oscillations were encountered.

case the bypass valves were closed and the flow rate was adjusted with the inlet valve. The method for the calculation is given in the Appendix. The result of the calculation is given in Fig. 12. Here the external pressure drop is taken as the pressure drop across the pump and the internal pressure drop as that from the outlet to the inlet of the pump through the test loop. Since the pump used in the experiment is capable of large flow rate, the external pressure-drop vs flow-rate curve becomes flat in the range of flow rate concerned. The curves for the internal pressure drop have a negative slope region, thus a flow excursion is predicted to occur at the heat flux of 1.5 MW m^{-2} and the mass velocity of 1750 kg m^{-2} s^{-1}, which are in good agreement with the measured CHF and mass velocity, 1.47 MW m^{-2} and 1749 kg m^{-2} s^{-1}, respectively.

Another example is for the density-wave oscillation. Typical traces for this instability are presented in Fig. 5(b), and the predicted internal pressure-drop curves are shown in Fig. 13. The internal pressure-drop curves have a positive slope in this case because of large inlet throttling, thus no flow excursion is expected. The burnout point marked with cross-in-circle is at the mass velocity 477 kg m^{-2} s^{-1} on the curve for the CHF 1.44 MW m^{-2}, whereas the predicted operating point at that heat flux is at the mass velocity 440 kg m^{-2} s^{-1}. The stability boundary of the density wave oscillation can be obtained from the simple criterion of Ishii and Zuber [32], as given by

$$x_e < \frac{2\left(K_i + \frac{f_m L}{2D} + K_e\right)}{1 + \frac{1}{2}\left(\frac{f_m L}{2D} + 2K_e\right)} \frac{\rho_g}{\Delta\rho}, \tag{4}$$

where the two-phase friction factor f_m can be calculated from the following equation:

$$\frac{f_m L}{2D} = \frac{\rho_l}{G^2} \Delta p_{TPF}, \tag{5}$$

where Δp_{TPF} is given by equation (A12).

Equations (4) and (5) predict for the case given in Fig. 13 that the density wave oscillations occur when the exit quality is larger than 0.025 at heat flux 1.44 MW m^{-2}. Since the exit quality at burnout is 0.194, the density wave oscillations are likely to occur in the case shown in Fig. 13.

Somewhat more complex flow oscillations, as shown in Fig. 9, were observed in the test section with the upstream compressibility and with the bypass fully open. According to the analysis on the pressure-drop oscillations by Maulbetsch and Griffith [18], the internal pressure drop is calculated as the pressure drop in the portion downstream of the compressible volume. The external pressure drop is calculated as the pump head minus the pressure drop from the outlet of the pump to the compressible volume. The resultant

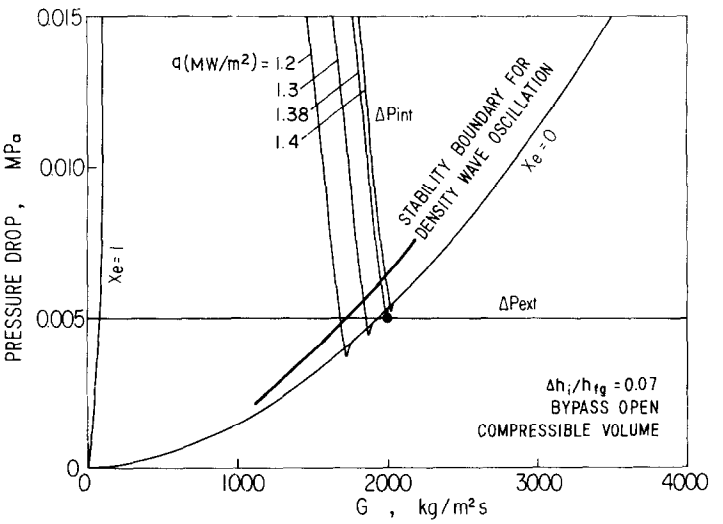

FIG. 14. Example of the pressure-drop vs flow-rate curves for the case shown in Fig. 9.

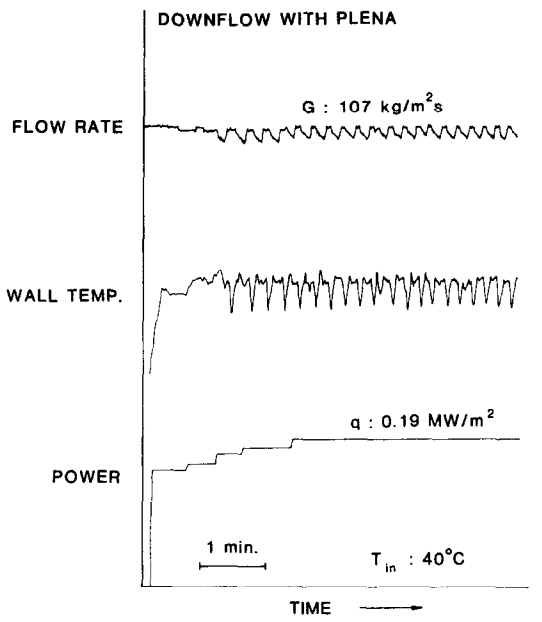

FIG. 15. Periodic flow oscillations observed in downflow at low mass velocities in the test section with an upper plenum.

pressure-drop vs flow-rate curves are as shown in Fig. 14. Maulbetsch and Griffith [18] pointed out that when the compressible volume was significantly large, the instability always occurred at the minimum in the pressure-drop vs flow-rate curve, leading to a burnout as a consequence. Therefore, it is expected in this case that the flow instability occurs at the point marked with solid circle in Fig. 14, at which point the mass velocity is $1990\,kg\,m^{-2}s^{-1}$ and the heat flux $1.38\,MW\,m^{-2}$. These values are reasonably close to the measured heat flux, $1.23\,MW\,m^{-2}$ and the mass velocity $1928\,kg\,m^{-2}s^{-1}$ at the onset of instability. The stability boundary for the density wave oscillations predicted by equation (4) is also shown with the bold line in Fig. 14. It is indicated that the operating point enters the region where the density-wave oscillations are likely to occur, after the onset of flow instability. It appears that the stored energy in the compressible volume worked to restore the flow rate. Therefore, the predominant mode of instability may be the pressure-drop oscillations followed by the density wave oscillations.

In the downflow experiment conducted with the upper plenum, periodic, low frequency oscillations were encountered, as depicted in Fig. 15. The period of the oscillations varied from several seconds to a few minutes which decreased with increasing mass velocity. In this case, the upper plenum may have served as an energy storage mechanism for the sustained oscillation. Predicted pressure-drop vs flow-rate curves are given in Fig. 16. The external pressure drop was calculated as the pump head minus the pressure loss from the outlet of the pump to the inlet of the upper plenum. The operating point marked with solid circle which is close to the condition observed at the occurrence of burnout is in the negative slope region on the pressure-drop vs flow-rate curve. Therefore, this may be a pressure-drop oscillation, though it is considerably affected by the buoyancy acting on the bubbles particularly at low mass velocities.

Relation between the CHF and the stability boundaries. In this section, observed stability boundaries are compared to the CHF data in order to provide a better understanding of burnout mechanisms. In Fig. 17, the stability boundaries both for upflow and downflow under stiff conditions are plotted in terms of non-dimensional heat flux vs mass velocity defined as follows:

$$q^* = q/(h_{fg}\sqrt{\lambda\rho_g g\Delta\rho}), \tag{6}$$

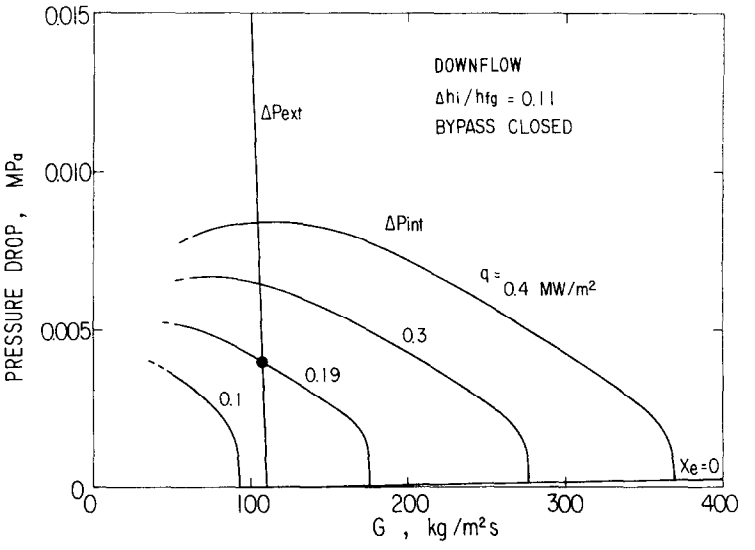

FIG. 16. Pressure-drop vs flow-rate curves for the case shown in Fig. 15.

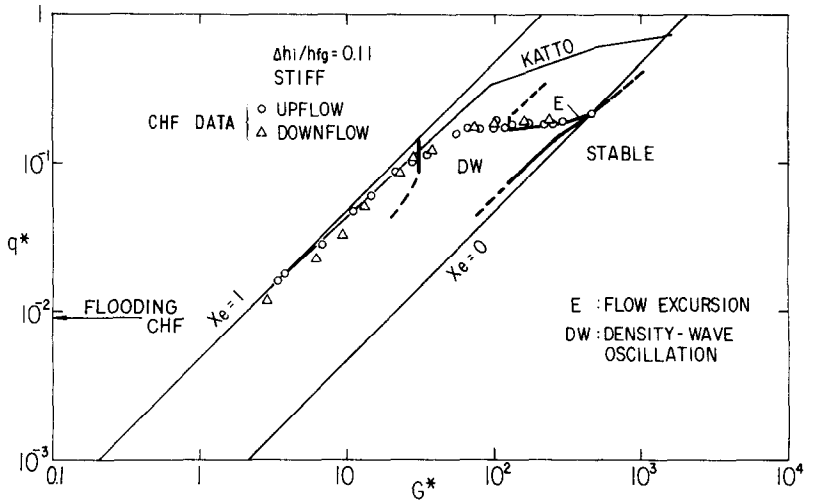

FIG. 17. Stability boundaries for upflow and downflow under stiff condition.

$$G^* = G/\sqrt{\lambda \rho_g g \Delta\rho}, \tag{7}$$

where

$$\lambda = \sqrt{\sigma/(g\Delta\rho)}. \tag{8}$$

The bold lines in Fig. 17 represent the stability boundaries. The density wave oscillations are observed in the region denoted by DW while the flow excursion occurs only on the line marked with E, because the onset of flow excursion directly results in burnout. The straight line denoted by $x_e = 0$ represents the location where the exit equilibrium quality becomes zero while the one denoted by $x_e = 1$ represents the location where the exit equilibrium quality becomes unity. Thus, the bulk flow is subcooled in the region below the line with $x_e = 0$ and all the liquid is evaporated in the region above the line with $x_e = 1$ in view of thermal equilibrium. The measured CHF data are plotted with circles and triangles. The Katto correlation [11] is also shown in Fig. 17 as a reference for stable-flow high-quality CHF in round tubes.

The results shown in Fig. 17 can be summarized as follows:

(1) At low mass velocities, the flow is stable or the onset of flow instability is not obvious. Typical traces under such conditions have been shown in Fig. 5(a). The CHF in upflow is well correlated by the stable-flow high-quality CHF correlation, while the CHF in downflow is as much as 30% lower than that in upflow. This may be attributed to the buoyancy effect acting on the bubbles.

(2) At higher mass velocities, however, the density-wave oscillations with large amplitudes, as given in Fig. 6, are encountered and the CHF decreases considerably from the stable-flow CHF. The traces for this case have been shown in Fig. 5(b).

(3) As the mass velocity further increases, the density-

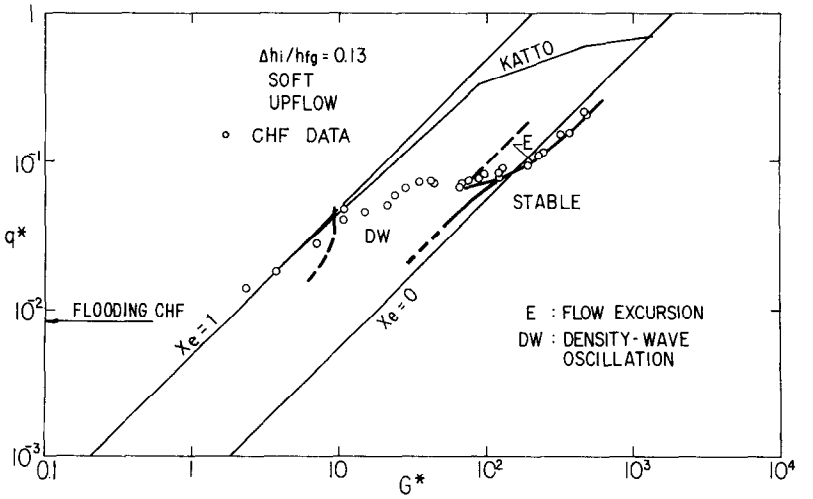

FIG. 18. Stability boundaries for upflow under soft condition.

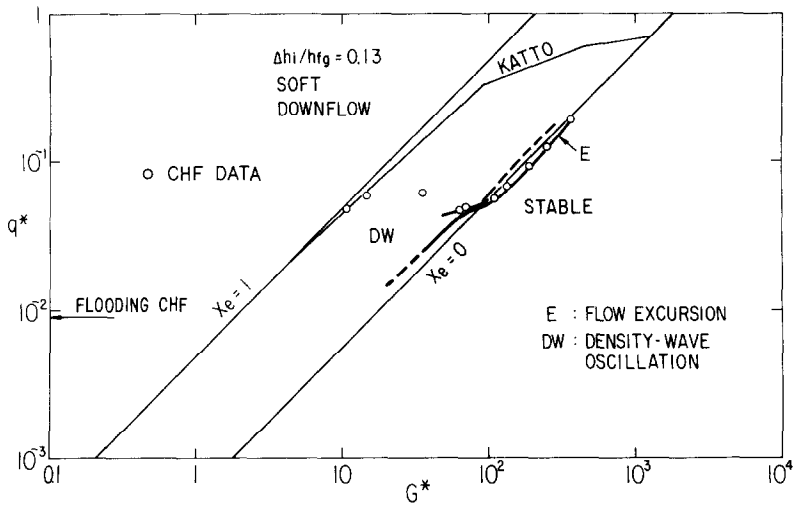

FIG. 19. Stability boundaries for downflow under soft condition.

wave oscillations are followed by the flow excursion which directly leads to burnout.

(4) At the highest mass velocities where the exit quality is near zero or slightly negative, the flow excursion occurs with no obvious preceding density-wave oscillations. It should be noted that this condition for the exit quality approximately agrees with the minimum in the internal pressure drop vs flow-rate curve.

A similar stability map is obtained for upflow in the soft system and in the test section with the upstream compressibility. An example is shown in Fig. 18 for upflow in the soft system. It can be seen from the comparison between Figs. 17 and 18 that the boundaries are moved toward lower heat flux and mass velocity in the soft system, and that the more unstable the flow is, the lower the CHF.

The stability boundaries for downflow in the soft system are shown in Fig. 19, which is very similar to that for corresponding upflow case, although the downflow appears to be less stable than the upflow.

When the upper plenum serves as a large upstream compressibility in downflow, a different stability map is obtained, as illustrated in Fig. 20. The pressure-drop oscillations, sometimes mixed with the density-wave oscillations, are observed prior to the burnout. The stability boundary is close to the line for zero exit quality. The CHF is also close to the same line at higher mass velocities, which agrees with the observation by Maulbetsch and Griffith [18]. The CHF at lower mass velocities in this case is remarkably reduced due to unstable flow and rather close to the flooding CHF or to the annular-flow boundary which can be approximated by the following equation [33]:

$$q^* = q^*_{cF} + \frac{A}{A_H}\frac{\Delta h_i}{h_{fg}} G^*, \tag{9}$$

where q^*_{cF} is the non-dimensional flooding CHF. In the

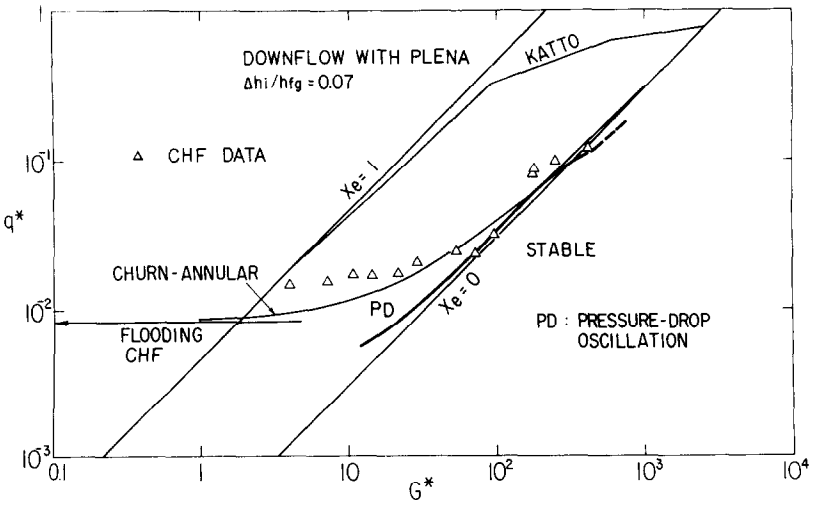

FIG. 20. Stability boundaries for downflow with an upper plenum.

present case q^*_{cF} is determined from the measured CHF at zero inlet mass velocity.

4. CONCLUSIONS

The results obtained from the present study are summarized as follows:

(1) The stable-flow CHF at low mass velocities can be well correlated by the conventional high-quality correlations, such as the Katto correlation [11]. In downflow, however, the CHF is as much as 30% lower than the upflow CHF at very low mass velocities due to the effect of buoyancy.

(2) The CHF at intermediate exit qualities appears to be significantly affected by the density-wave oscillations. The flow becomes more unstable by providing upstream compressibility, less inlet throttling and bypass, which cause a substantial reduction of CHF.

(3) Due to the buoyancy effect the downflow is less stable than the upflow. Particularly when the test section has an upper plenum, the latter works as an effective upstream compressibility to induce the pressure-drop oscillations. The CHF in this case is kept almost constant at very low heat flux until the mass velocity exceeds the critical value to stagnate rising bubbles or the value corresponding to zero exit quality.

(4) At higher mass velocities, the lines for the above mentioned unstable CHF intersect the zero-exit-quality line around which the minimum in the internal pressure-drop vs flow-rate curve occurs. Beyond this mass velocity, the CHF increases along the line for zero exit quality, irrespective of the flow orientation. In this regime, CHF occurs mainly due to flow excursion.

(5) There appears to be a minimum CHF as a function of mass velocity, which occurs due to flooding. It turned out that all the data which suffered flow instabilities fall in the region which was bounded by the stable-flow CHF lines, the flooding CHF line or the annular-flow boundary, and the line corresponding to the minimum in the internal pressure-drop vs flow-rate curve.

From these results, it may be concluded that the CHF at low flow rate and low pressure conditions is largely affected by various flow instabilities. At lower heat flux, the basic mechanism of burnout will be the dryout or breakdown of the liquid film on the heated surface, which is caused by the deficiency of the liquid in the heated section and may be controlled by such hydrodynamical phenomena as flooding or flow reversal, entrainment and deposition of liquid droplets. Such flow instabilities as the density-wave oscillations, the pressure-drop oscillations and the flow excursion can reduce the effective film flow rate, thus leading to premature burnout.

When both the mass velocity and the heat flux are high, and the exit quality is near zero, the flow excursion appears to be the dominant phenomenon to cause burnout. The flow excursion leads to total liquid starvation and causes dryout over a wide area of the heated surface. When the heat flux is sufficiently high, say, higher than the pool-boiling CHF, a temporary reduction of flow rate due to flow instability would initiate vapor-blanketing which can not be quenched by the subsequent increase of the flow rate. In that case, a DNB-type burnout will result.

Acknowledgements—This work was supported by the Grant-in-Aid for Scientific Research No. 58124030 (1983) from the Ministry of Education, Science and Culture of Japan. The authors would like to express their thanks to Professor T. Shibata of Research Reactor Institute of Kyoto University for his support and encouragement in this work. Thanks are also extended to Mr N. Yagoro for his assistance in the experiment.

REFERENCES

1. W. R. Gambill, Burnout in boiling heat transfer—Part I: Pool boiling systems, *Nucl. Safety* **9**, 351–362 (1968).
2. W. R. Gambill, Burnout in boiling heat transfer—Part II: Subcooled forced-convection systems, *Nucl. Safety* **9**, 467–480 (1968).
3. A. E. Bergles, Burnout in boiling heat transfer. Part I: Pool boiling systems, *Nucl. Safety* **16**, 29–42 (1975).
4. A. E. Bergles, Burnout in boiling heat transfer. Part II: Subcooled and low-quality forced-convection systems, *Nucl. Safety* **18**, 154–167 (1977).
5. A. E. Bergles, Burnout in boiling heat transfer. Part III: High-quality systems, *Nucl. Safety* **20**, 671–689 (1979).
6. V. Marinelli, Critical heat flux: a review of recent publications, *Nucl. Technology* **34**, 135–171 (1977).
7. L. S. Tong, *Boiling Heat Transfer and Two-phase Flow*. John Wiley, New York (1965).
8. J. G. Collier, *Convective Boiling and Condensation*. McGraw-Hill, London (1972).
9. R. V. Macbeth, Burnout analysis, Part IV, application of a local conditions hypothesis to world data for uniformly heated tubes and rectangular channels, AEEW-R267 (1963).
10. B. Thompson and R. V. Macbeth, Boiling water heat transfer burnout in uniformly heated round tubes: a compilation of world data with accurate correlations, AEEW-R356 (1964).
11. Y. Katto, A generalized correlation of critical heat flux for the forced convection boiling in vertical uniformly heated round tubes, *Int. J. Heat Mass Transfer* **21**, 1527–1542 (1978).
12. Y. Katto, An analytical investigation of CHF of flow boiling in uniformly heated vertical tubes with special reference to governing dimensionless groups, *Int. J. Heat Mass Transfer* **25**, 1353–1361 (1982).
13. D. A. Barnard, F. R. Dell and R. Stinchcombe, R.S.100: dryout at low mass velocities for an upward boiling flow of refrigerant-113 in a vertical tube, AERE-R7726 (1974).
14. W. H. Lowdermilk, C. D. Lanzo and B. L. Siegel, Investigation of boiling burnout and flow stability for water flowing tubes, NACA-TN 4382 (1958).
15. V. I. Aladiev, Z. L. Miropolsky, V. E. Doroschuk and M. A. Styrikovich, Boiling crisis in tubes, *Proceedings of the International Heat Transfer Conference*, ASME (1961).
16. A. E. Bergles, Subcooled burnout in tubes of small diameter, ASME Paper No. 63-WA-182 (1963).
17. R. S. Daleas and A. E. Bergles, Effects of upstream compressibility on subcooled critical heat flux, ASME Paper No. 65-HT-67 (1965).
18. J. S. Maulbetsch and P. Griffith, System-induced instabilities in forced convection flows with subcooled boiling, *Proceedings of the Third International Heat Transfer Conference*, Chicago, Vol. 4, pp. 247–257 (1966).
19. A. E. Bergles, R. F. Lopina and M. P. Fiori, Critical-heat flux and flow-pattern observations for low-pressure water flowing in tubes, *J. Heat Transfer* **89**, 69–74 (1967).

20. F. Mayinger, O. Schad and E. Weiss, Research into the critical heat flux (burnout) in boiling water, EURAEC-1620 (1966).
21. D. B. Collins, M. Gacesa and C. B. Parsons, Study of onset of premature heat transfer crisis during hydrodynamic instability in a full-scale reactor channel, ASME Paper No. 71-HT-11 (1971).
22. A. R. Blumenkrantz and W. R. Gambill, Buoyancy effects on thermal burnout with downflow of water in vertical channels, as appeared in ref. [2].
23. M. Cumo, R. Bertoni, R. Cipriani and G. Palazzi, Upflow and downflow burnout, *Inst. Mech. Engrs Conference Publications*, 1977–8, pp. 183–192 (1977).
24. G. J. Kirby, R. Staniforth and J. H. Kinneir, A visual study of forced convection boiling, Part 2. Flow patterns and burnout for a round test section, AEEW-R506 (1967).
25. K. Mishima and H. Nishihara, Critical heat flux at low-flow-rate and low-pressure conditions in thin rectangular channels, to be published.
26. M. Ishii, One-dimensional drift-flux model and constitutive equation for relative motion between phases in various two-phase flow regimes, ANL-77-47 (1977).
27. J. A. Bouré, A. E. Bergles and L. S. Tong, Review of two-phase flow instability, *Nucl. Engng Des.* **25**, 165–192 (1973).
28. M. Ishii, Study on flow instabilities in two-phase mixtures, ANL-76-23 (1976).
29. S. Kakaç and T. N. Veziroglu, A review of two-phase flow instabilities. In *Advances in Two-phase Flow and Heat Transfer* (Edited by S. Kakaç and M. Ishii), Vol. II, pp. 577–667. Martinus Nijhof (1983).
30. M. Ledinegg, Instability of flow during natural and forced circulation, *Wärme* **61**, 8 (1938).
31. M. Ishii and H. K. Fauske, Boiling and dryout behavior in a liquid–metal fast breeder reactor subassembly bundle under low heat flux and low flow conditions, *Nucl. Sci. Engng* **84**, 131–146 (1983).
32. M. Ishii and N. Zuber, Thermally induced flow instabilities in two-phase mixtures, *Proceedings of the Fourth International Heat Transfer Conference*, Paris, Paper No. B5.11 (1970).
33. K. Mishima and M. Ishii, Critical heat flux experiments under low flow conditions in a vertical annulus, ANL-82-6 (1982).

APPENDIX

Resistance coefficient of the inlet valve

As the pressure drops across the test section and the inlet valve were not measured, they were estimated by using the known pump characteristic and measured single-phase flow rate after shutting down the power to the test section due to burnout. This is proper because the valve opening is not changed before and after the burnout.

Since the resistance coefficient of the flowmeters were known, the resistance coefficient of the inlet valve can be calculated assuming the following form

$$\Delta p_{ext}(G) = \Delta p_{ini}(G), \tag{A1}$$

where

$$\Delta p_{ext}(G) = \Delta p_{pump}(G), \tag{A2}$$

$$\Delta p_{ini}(G) = K_i \frac{G^2}{\rho_i} + \frac{f_i G^2}{2D\rho_i}(L_H + L_u) + K_e \frac{G^2}{\rho_i}. \tag{A3}$$

Here the first term on the RHS represents the inlet pressure loss which includes the resistances at the flowmeter and the inlet valve as well as the pressure loss in the inlet pipe. The second term is the frictional pressure loss in the heated and upper unheated sections, and the third term the exit pressure loss.

The exit resistance coefficient K_e is chosen as 0.5 and the inlet resistance coefficient K_i determined from the experiment. The single phase friction factor f_i is obtained from

$$f_i = 0.3164\, Re_i^{-0.25}, \tag{A4}$$

where

$$Re_i = GD/\mu_i. \tag{A5}$$

Two-phase pressure drop

Two-phase pressure drop is given by

$$\Delta p_{int} = K_i \frac{G^2}{\rho_{ii}} + \frac{f_i G^2 L_{NB}}{2D\rho_{ii}} + \Delta p_{TPF} + \Delta p_g + \Delta p_e + \Delta p_A. \tag{A6}$$

The exit pressure loss Δp_e can be calculated by [8]

$$\Delta p_e = K_e\left(1 + \frac{\Delta\rho}{\rho_g} x_e^{1.5}\right)\frac{G^2}{\rho_{ii}}, \tag{A7}$$

where the exit quality is

$$x_e = \frac{4Lq}{h_{fg}DG} - \frac{\Delta h_i}{h_{fg}}. \tag{A8}$$

The gravity term Δp_g is approximated by

$$\Delta p_g = -\Delta\rho g\alpha_H(L_H - L_{NB}) - \Delta\rho g\alpha_e L_u, \tag{A9}$$

where α_H is the average void fraction in the boiling region and α_e the void fraction at the exit of the heated section. The void fraction at the exit of the heated section can be calculated by

$$\alpha_e = \frac{1}{1 + \dfrac{1-x_e}{x_e}\dfrac{\rho_g}{\rho_l}}. \tag{A10}$$

It is assumed that the average void fraction α_H is calculated using the average quality in the heated section and from the homogeneous flow model, hence,

$$\alpha_H = \frac{1}{1 + \dfrac{1-0.5x_e}{0.5x_e}\dfrac{\rho_g}{\rho_l}}. \tag{A11}$$

The above simplification turned out to produce no significant errors in the final results for the present case. Another simplification is to assume that the acceleration term Δp_A can be neglected because it is cancelled out due to condensation in the downstream of the loop, as stated by Ishii *et al.* [31]. Approximate equation for the two-phase friction terms was also given by Ishii *et al.* [31] based on the homogeneous-flow model and is expressed as

$$\Delta p_{TPF} = \frac{f_l G^2}{2D\rho_{li}}\left[\left(1 + \frac{\Delta\rho}{\rho_g}\frac{x_e}{2}\right)(L_H - L_B)\left(1 + \frac{\Delta\mu}{\mu_g}\frac{x_e}{2}\right)^{-0.25} + \frac{\left(1 + \dfrac{\Delta\rho}{\rho_g}x_e\right)L_u}{\left(1 + \dfrac{\Delta\mu}{\mu_g}x_e\right)^{0.25}}\right]. \tag{A12}$$

ASSECHEMENT ET INSTABILITES D'ECOULEMENT POUR L'EAU BOUILLANTE DANS UN TUBE CIRCULAIRE, A PRESSION ATMOSPHERIQUE

Résumé—Pour étudier le flux thermique critique (CHF) aux faibles débits masses, les conditions d'arrêt d'écoulement et de renversement, une expérience est conduite avec de l'eau en écoulement dans un tube circulaire à pression atmosphérique. L'attention principale est portée sur les effets de gravité (écoulement ascendant ou descendant), la compressibilité et le laminage à l'entrée. Les résultats indiquent que le CHF dû aux instabilités peut être fortement inférieur à celui de l'écoulement stable. On montre aussi que la limite inférieure du CHF d'écoulement instable correspond à la limite du CHF dans l'écoulement annulaire.

BURNOUT UND STRÖMUNGSINSTABILITÄTEN BEIM SIEDEN VON STRÖMENDEM WASSER IN EINEM ROHR UNTER ATMOSPHÄRENDRUCK

Zusammenfassung—Im Rahmen der Untersuchung der kritischen Wärmestromdichte (CHF) bei kleinen Strömungsgeschwindigkeiten, bei Strömungsstagnation und Strömungsumkehrbedingungen wurden Experimente mit strömendem Wasser in einem Rohr unter Atmosphärendruck durchgeführt. Hauptsächlich betrachtet wurden Auftriebseffekte (d. h. Aufwärts- und Abwärtsströmung), Kompressibilität und Drosselung durch ein Einlaßventil. Die Ergebnisse zeigen, daß die kritische Wärmestromdichte—verursacht durch Strömungsinstabilitäten—beträchtlich geringer sein kann als bei stabiler Strömung. Außerdem ist die untere Grenze der kritischen Wärmestromdichte bei instabiler Strömung gleich der bei Ringströmung oder beim Überfluten.

НЕУСТОЙЧИВОСТИ КИПЕНИЯ И ТЕЧЕНИЯ ВОДЫ, ДВИЖУЩЕЙСЯ В КРУГЛОЙ ТРУБЕ ПРИ АТМОСФЕРНОМ ДАВЛЕНИИ

Аннотация—Для изучения критического теплового потока (КТП) при низких массовых скоростях и при условиях торможения течения и изменения направления течения был проведен эксперимент с водой, движущейся в круглой трубе при атмосферном давлении. Основное внимание уделено действию подъемной силы (т.е. восходящему и нисходящему потокам), учету сжимаемости вверх по течению и условиям на входе. Результаты показали, что из-за неустойчивостей течения КТП может быть значительно ниже, чем при устойчивом течении. Также показано, что более низкая граница КТП при неустойчивом течении наблюдается в кольцевом канале.